Intrinsic anisotropy of degree of transport spin polarization in typical ferromagnets

2008 J. Phys.: Condens. Matter 20 275245

(http://iopscience.iop.org/0953-8984/20/27/275245)

J. Phys.: Condens. Matter **20** (2008) 275245 (8pp) doi:10.1088/0953-8984/20/27/275245

Intrinsic anisotropy of degree of transport spin polarization in typical ferromagnets

Z Y Zhu[1], H W Zhang[1], S F Xu[1], J L Chen[1], G H Wu[1], B Zhang[2] and X X Zhang[2]

[1] Beijing National Laboratory for Condensed Matter Physics, Institute of Physics, Chinese Academy of Sciences, Beijing 100080, People's Republic of China
[2] Department of Physics and Institute of Nanoscience and Technology, The Hong Kong University of Science and Technology, Clear Water Bay, Kowloon, Hong Kong, People's Republic of China

E-mail: ghwu@aphy.iphy.ac.cn

Received 26 October 2007, in final form 28 April 2008
Published 13 June 2008
Online at stacks.iop.org/JPhysCM/20/275245

Abstract

A general approach is presented for investigation of the anisotropy of the degree of transport spin polarization (P) in ferromagnets both in the ballistic regime, $P_{1,i}$, and in the diffusive regime, $P_{2,i}$, as a function of crystal direction. The validity of this approach is confirmed by the benchmark calculation for the isotropic P. By this approach, we have investigated the anisotropy of P in bcc Fe, fcc Co, fcc Ni and hcp Co. For cubic structures, $P_{1,i}$ shows a small but appreciable anisotropy, due to the difference in the electronic orbital extension for spin-up and spin-down conduction bands. However, $P_{2,i}$ shows an isotropic feature for the cubic structure, as a result of the combination of its dependence on the square of electron velocity and the lattice symmetry. On the other hand, for hcp Co, both $P_{1,i}$ and $P_{2,i}$ show a very strong anisotropy. The large anisotropy of $P_{1,i}$ and $P_{2,i}$ in hcp Co is mainly attributed to the anisotropy of spin-down ballistic (diffusive) conductance.

1. Introduction

Since the discovery of giant magnetoresistance (GMR) and tunneling magnetoresistance (TMR), the topic of spintronics has been intensively investigated because of its increasing application to magnetic recording devices [1–5]. Despite the differences in the configurations of various systems, they are commonly characterized by the transfer or injection of a spin polarized current from a ferromagnetic component into a nonmagnetic metal or semiconductor [6, 7]. For such a spin dependent transport, it is highly important for the available spin-up and spin-down conductive electrons near the Fermi level to have a relatively asymmetrical conductivity. Therefore, the so-called degree of transport spin polarization (P) that describes the extent of asymmetry of the spin polarized transport current is one of the most important parameters to determine the size of magnetoresistance. The reported values of P have ranged from about 40% for a conventional ferromagnetic material, such as Fe, to almost 100% in the so-called half metallic materials [3, 8, 9]. In the latter case, the transport current is ideally carried by only spin-up or spin-down electrons. Some Heusler alloys, half Heusler alloys and simple metallic oxides have been identified as half metals by electronic structure calculations, and subsequently high values of P have also been discovered in these materials [9–12].

Different techniques, such as spin polarized photoemission [13], point contact Andreev reflection [8] and tunneling junction [14], are used to measure P for ferromagnetic materials. For the so-called half metals, spin polarization of these special materials is theoretically independent of the various experimental methods. The reason is that only one spin channel has available states at the Fermi level and hence all current must be carried only by spin-up (or spin-down) electrons. So P in the half metal should always be expected to be 100%. However, for a regular ferromagnet, both the spin-up and spin-down electrons make contributions to the total current. Therefore, it is necessary for P to be defined in several different ways in order to explain the results from the various kinds of experiments. Assuming that spin-flip scattering does not exist, the current in each spin channel is considered to be dependent only on the characteristics of each corresponding spin subsystem,

and hence the definition of P can be expressed as follows [15]:

$$P_n = \frac{\langle N(E_F)v_F^n\rangle_\uparrow - \langle N(E_F)v_F^n\rangle_\downarrow}{\langle N(E_F)v_F^n\rangle_\uparrow + \langle N(E_F)v_F^n\rangle_\downarrow} \quad (1)$$

where N and $\boldsymbol{v}_F$ are electronic density of states and Fermi velocity, respectively, $\uparrow$ ($\downarrow$) stands for spin-up (spin-down) channel and $\langle\,\rangle$ denotes the integration over the whole Fermi surface.

In the spin polarized photoemission experiment, the conductivity of each spin channel is proportional to the electronic density of states of each corresponding spin channel and independent of the electronic velocity of the electrons [13]. So the definition of P with $n = 0$, P_0, is appropriate for the spin polarized photoemission experiment. However, in the cases of point contact Andreev reflection and tunneling junction, both the velocity of the conductive electrons and the electronic density of states make contributions to the conductivity. Therefore, the inclusion of the Fermi velocity in the description of the conductivity of each spin channel is necessary for the definition formula of P. When the size of the contact is much smaller than the mean free path of the electrons, the electrons can flow through the contact ballistically. For such purely ballistic regime, the conductivity of each spin channel is proportional to $\langle Nv\rangle_\sigma$ (σ is $\uparrow$ or $\downarrow$ for spin-up and spin-down channels, respectively.) in the Fermi sphere approximation [15, 16]. If considering the arbitrary Fermi surface geometry, however, the conductivity of each spin channel is proportional to $\langle Nv\rangle_\sigma$ and $\langle Nv^2\rangle_\sigma$, for a ballistic contact with no barrier and a large barrier, respectively. On the other hand, when the size of the contact is larger than the mean free path of the electrons, the electronic transport lies in the diffusive regime. Under this circumstance, the conductivity of each spin channel is proportional to $\tau_\sigma \frac{n_\sigma}{m_\sigma}$, according to the Drude theory. τ_σ is the relaxation time and $\frac{n_\sigma}{m_\sigma}$ is sometimes expressed as $\langle Nv^2\rangle_\sigma$ and is proportional to the contribution of the corresponding electrons to the plasma frequency [17]. Therefore, if we assume the same relaxation time in both spin channels, the conductivity of each spin channel in the diffusive regime is proportional to $\langle Nv^2\rangle_\sigma$. Therefore, according to the definition formula, for low resistance ballistic contacts, P_1 is appropriate and the definition of P_2 corresponds to a large barrier and/or diffusive current [15].

Unlike scalar N, the electronic velocity $\boldsymbol{v}$ is a vector. Therefore, $\langle Nv\rangle$ and $\langle Nv^2\rangle$ should vary with crystal directions, especially for the materials with noncubic symmetry. In other words, both $\langle Nv\rangle$ and $\langle Nv^2\rangle$ are anisotropic, which has been verified experimentally by the ratio of conductivity in the [100] direction to that in the [001] direction being 1.84 rather than 1 [18]. Furthermore, for the spin dependent transport, the intrinsic anisotropy of magnetoresistance induced by the pure band effects has been reported in some papers [19–21]. Therefore, like in the case of conductivity, the intrinsic anisotropy of P_1 and P_2 can NOT be neglected in the investigation on spin dependent transport properties, if the relative difference between the projections of $\boldsymbol{v}_F$ for spin-up and spin-down channels on a certain crystal direction is much larger than that on the other directions. Compared with the conventional definition P_0, P_1 and P_2 should be much more complicated because of the inclusion of $\boldsymbol{v}$ in the description of electronic mobility. According to the definitions of P_1 and P_2 in (1), the anisotropic P can be written as a function of crystal direction i:

$$P_{n,i} = \frac{\langle N(E_F)v_{F,i}^n\rangle_\uparrow - \langle N(E_F)v_{F,i}^n\rangle_\downarrow}{\langle N(E_F)v_{F,i}^n\rangle_\uparrow + \langle N(E_F)v_{F,i}^n\rangle_\downarrow} \quad (2)$$

here, $v_{F,i}$ stands for the projection of $\boldsymbol{v}_F$ on i direction. $n = 1$ and 2 are in accordance with the cases in ballistic and diffusive regimes, respectively. For clarity, hereinafter in this paper, the P defined by (2) are called the anisotropic $P_{1,i}$ and $P_{2,i}$, and the P defined by (1) are called isotropic P_0, P_1 and P_2.

Recently, an approach based on the so-called tetrahedron method has been reported [22] to calculate P under the isotropic definition in both ballistic and diffusive limits. In that report, the anisotropic distribution of the electronic velocity vectors in real space is neglected. However, as stated above, the intrinsic anisotropy of P in both ballistic and diffusive regimes should be an important phenomenon, especially in the noncubic compound. So the calculation of anisotropic $P_{1,i}$ and $P_{2,i}$ is expected for the deeper understanding of the spin dependent transport properties in ferromagnets with both cubic and noncubic lattices. In this paper, we present a general approach to evaluate $P_{1,i}$ and $P_{2,i}$ with high accuracy. Details of the approach are explained in section 2. We calculate the anisotropic $P_{1,i}$ and $P_{2,i}$ of body-centered cubic (bcc) Fe, face-centered cubic (fcc) Co, fcc Ni and hexagonal-close-packed (hcp) Co. Related results and discussions are given in section 3. Additionally, at the beginning of this section, the calculating method is validated by the benchmark calculation for isotropic P_0, P_1 and P_2 of bcc Fe and fcc Ni, in which the anisotropic distribution of the electronic velocity vectors in real space is neglected [22]. The conclusions are drawn in section 4.

2. Methodology

To calculate $\langle N(E_F)v_F^n\rangle_\sigma$ ($\sigma = \uparrow$ and $\downarrow$ for spin-up and spin-down channel, respectively) for the isotropic P_0, P_1 and P_2 as given in (1), the following expression is used:

$$\begin{aligned}&\langle N(E_F)v_F^n\rangle_\sigma \\ &= \frac{1}{(2\pi)^3}\sum_\lambda \int v_{F,\boldsymbol{k},\lambda,\sigma}^n \delta(E_{\boldsymbol{k},\lambda,\sigma} - E_F)\,\mathrm{d}^3k \\ &= \frac{1}{(2\pi)^3}\sum_\lambda \int v_{F,\boldsymbol{k},\lambda,\sigma}^{n-1}\,\mathrm{d}S_F \end{aligned} \quad (3)$$

here $\boldsymbol{k}$, λ and σ denote wavevector, band and spin indexes, respectively. $E_{\boldsymbol{k},\lambda,\sigma}$ stands for the electronic energy in the band λ with spin σ and the wavevector $\boldsymbol{k}$. $\mathrm{d}S_F$ stands for the area of an Fermi surface element.

Similarly, the form of $\langle N(E_F)v_{F,i}^n\rangle_\sigma$ in anisotropic $P_{1,i}$ and $P_{2,i}$ can be obtained by substituting $v_{F,\boldsymbol{k},\lambda,\sigma,i}^n$ for $v_{F,\boldsymbol{k},\lambda,\sigma}^n$ (the former is the projection of the latter on i direction) in (3) as:

$$\begin{aligned}&\langle N(E_F)v_{F,i}^n\rangle_\sigma \\ &= \frac{1}{(2\pi)^3}\sum_\lambda \int v_{F,\boldsymbol{k},\lambda,\sigma,i}^n \delta(E_{\boldsymbol{k},\lambda,\sigma} - E_F)\,\mathrm{d}^3k \\ &= \frac{1}{(2\pi)^3}\sum_\lambda \int \frac{v_{F,\boldsymbol{k},\lambda,\sigma,i}^n}{v_{F,\boldsymbol{k},\lambda,\sigma}}\,\mathrm{d}S_F. \end{aligned} \quad (4)$$

To obtain the dS_F in (3) and (4) for numerical calculation, the Fermi surface should be first divided into large number of surface elements to make their areas very small; next the precondition of electrons with the same velocity is satisfied within a allowable tolerance in this area. Subsequently, the energy gradient of the electron in this area should be calculated in the reciprocal space to evaluate the Fermi velocity in (3) and its projection on the i direction in (4). In the following paragraph, we will present details of the said steps.

As a kind of isosurface in the reciprocal space, the Fermi surface can be obtained using the so-called Marching Cubes Algorithm [23], in which Fermi energy is regarded as the isovalue. As described in [24], the obtained Fermi surface is composed of many triangles. If the number of grid points for the input energy data is large enough, the number of triangles in a Fermi surface will also be big enough. So, the area of this kind of triangle can be used as the area element dS_F in the evaluation of (3) and (4), and in the following the characters of the electrons in this area element will be represented by the character of the electron at the center of the triangle.

For an electron at the center of a triangle, its Fermi velocity projections on the three coordinate axes of the orthogonal coordinate system, $v_{F,a}$ ($a = x$, y and z) can be written as:

$$v_{F,a} = \frac{1}{\hbar}\left(\frac{\partial E}{\partial k_a}\right)_F = \frac{1}{2\hbar}\left(\frac{E_{k_F+\delta k_a} - E_F}{\delta k_a} + \frac{E_F - E_{k_F-\delta k_a}}{\delta k_a}\right)$$
$$= \frac{1}{2\hbar}\left(\frac{E_{k_F+\delta k_a} - E_{k_F-\delta k_a}}{\delta k_a}\right). \quad (5)$$

The energy values at (near) the center of this triangle, E_F ($E_{k_F\pm\delta k_a}$), can be obtained by linear interpolation of the energy values at the neighboring grid points. δk_a has been set to a small enough value in order to obtain $v_{F,a}$ with a satisfactory accuracy.

For crystal direction i([l, m, n]) and the basis vectors of the crystal structure ($\boldsymbol{r}_{[1,0,0]} = r_{a,x}\boldsymbol{i} + r_{a,y}\boldsymbol{j} + r_{a,z}\boldsymbol{k}$, $\boldsymbol{r}_{[0,1,0]} = r_{b,x}\boldsymbol{i} + r_{b,y}\boldsymbol{j} + r_{b,z}\boldsymbol{k}$ and $\boldsymbol{r}_{[0,0,1]} = r_{c,x}\boldsymbol{i} + r_{c,y}\boldsymbol{j} + r_{c,z}\boldsymbol{k}$), the projection of $\boldsymbol{v}_F$ on the i direction (i.e., a vector direction along the i direction, $\boldsymbol{r}_i/|\boldsymbol{r}_i|$), $v_{F,i}$, can be expressed as:

$$v_{F,i} = \frac{1}{|\boldsymbol{r}_i|}\boldsymbol{v}_F \cdot \boldsymbol{r}_i = \frac{1}{\sqrt{r_x^2 + r_y^2 + r_z^2}}$$
$$\times (v_{F,x} \cdot r_x + v_{F,y} \cdot r_y + v_{F,z} \cdot r_z) \quad (6)$$

where

$$\boldsymbol{r}_i = r_x\boldsymbol{i} + r_y\boldsymbol{j} + r_z\boldsymbol{k} \quad (7)$$

and

$$r_t = l \cdot r_{a,t} + m \cdot r_{b,t} + n \cdot r_{c,t}, \qquad (t = x, y, z). \quad (8)$$

Now, $\langle N(E_F)v_F^n\rangle_\sigma$ and $\langle N(E_F)v_{F,i}^n\rangle_\sigma$ can be found from the summation of all the contributing triangles on the Fermi surface of all the conduction bands, so various types of P can be calculated. It should be pointed out that in the case of $n = 1$, i.e. in the ballistic limit, the average over the whole Fermi surface should be zero because the spatial inversion symmetry demands $N(k) = N(-k)$ and $v(k) = -v(-k)$. In order to avoid a zero value of $\langle N(E_F)v_F\rangle_\sigma$ and $\langle N(E_F)v_{F,i}\rangle_\sigma$, we have only used terms with positive velocity values (i.e. $v_F > 0$ and $v_{F,i} > 0$) in the summation process.

Table 1. The isotropic P_0, P_1 and P_2 (in per cent) at the Fermi energy for bcc Fe, fcc Co and fcc Ni calculated in the present work. For comparison, the relevant values, which are obtained from previous works, are also listed.

bcc Fe			fcc Co			fcc Ni		
P_0	P_1	P_2	P_0	P_1	P_2	P_0	P_1	P_2
52.5[a]	36.1[a]	33.1[a]	−75.8[a]	−31.1[a]	21.7[a]	−79.6[a]	−43.0[a]	10.8[a]
60[b]	35[b]	24[b]				−80[b]	−49[b]	0[b]
54[c]	42[c]	37[c]				−80[c]	−47[c]	15[c]

[a] From the present work.
[b] From reference [15].
[c] From reference [22].

The last task is to produce the energy distribution in the first Brillouin zone by first-principles calculation. In this paper, for bcc Fe ($a = 2.866$ Å), fcc Co ($a = 3.544$ Å), fcc Ni ($a = 3.524$ Å) and hcp Co ($a = 2.507$ Å, $c = 4.069$ Å), the electronic structure calculations have been performed using the self-consistent full-potential linearized-augmented plane-wave method based on the local spin-density approximation within the density functional theory [25, 26]. The self-consistency is achieved at 455 k-points for bcc Fe, fcc Co and fcc Ni and 728 k-points for hcp Co in each irreducible Brillouin zone. To calculate the energy distribution in the reciprocal space, the first full Brillouin zone is divided into 125000 k meshes for bcc Fe, fcc Co and fcc Ni and 108 000 k meshes for hcp Co, respectively. An error of less than 2% has been obtained by a sufficiently large number of k meshes. The cutoff energy is set at 400 eV for all calculations.

3. Results and discussions

3.1. Isotropic P_0, P_1 and P_2 for bcc Fe, fcc Co and fcc Ni

For bcc Fe, fcc Co and fcc Ni, the calculated isotropic P_0, P_1 and P_2 as a function of the energy are shown in figure 1. First we focus on the values at the Fermi energy, which is relevant to the transport properties. In table 1, these values, as well as the values reported in previous papers [15, 22], are listed. For bcc Fe, the values of P_0, P_1 and P_2 at the Fermi energy are always positive despite the different weight of electronic velocity in the calculations. For fcc Co and fcc Ni, however, a kind of sign reversal from negative to positive values takes place from P_0 and P_1 to P_2 when the weight of electronic velocity becomes increasingly greater in the calculations. Considering the error caused by different approximations in electronic structure calculations [15], our results are in good agreement with those previous reports, which confirms the validity of the method in this work.

To understand fully the sign reversal in fcc Co and fcc Ni, we plot the spin polarized density of states for bcc Fe, fcc Co and fcc Ni in figure 2. As can be seen, around the Fermi energy, for fcc Co and fcc Ni their spin-up density of states shows an s-character, whereas their spin-down density of states show a d-character, as in the case of fcc Ni reported by Mazin [15]. Compared with a d-characterized electron, as is well known,

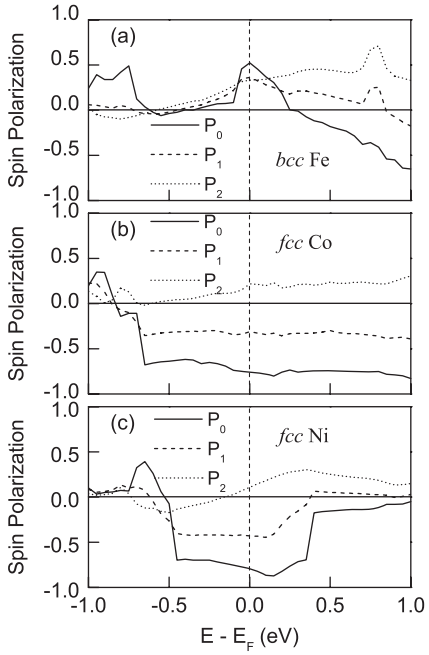

Figure 1. Calculated isotropic P_0, P_1 and P_2 for (a) bcc Fe, (b) fcc Co, and (c) fcc Ni.

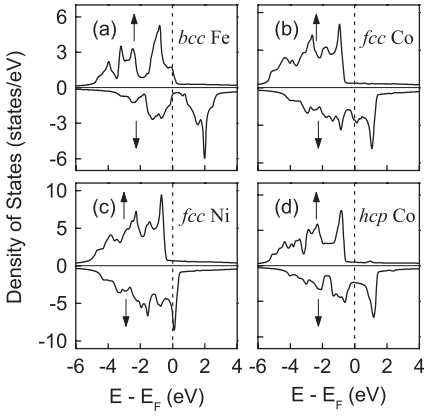

Figure 2. Spin polarized electronic density of states of (a) bcc Fe, (b) fcc Co, (c) fcc Ni, and (d) hcp Co. The up arrow and down arrow stand for spin-up and spin-down electrons, respectively.

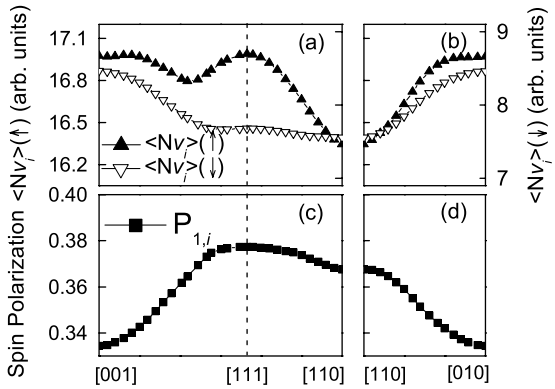

Figure 3. (a) and (b) Spin-up and spin-down ballistic conductance, $\langle Nv_i\rangle_\uparrow$ and $\langle Nv_i\rangle_\downarrow$, respectively, and (c) and (d) anisotropic $P_{1,i}$ as a function of the crystal direction i for bcc Fe.

an s-characterized one has much a larger velocity and smaller density of states, which means that the contribution of the spin-up channel to the total current is larger than that of the spin-down channel. Hence, sign reversals will take place when the weight of electronic velocity becomes increasingly greater. On the other hand, for bcc Fe, both spin-up and spin-down density of states show d-character at the Fermi energy and the density of states are large for both spins, which leads to the absence of the sign reversal in the case of bcc Fe. Thus, it is the different features between spin-up and spin-down conductive electrons that lead to the sign reversal. This phenomenon can also be found in the calculation for the anisotropic $P_{1,i}$ and $P_{2,i}$ as will be shown below. The comparison between figures 1 and 2 shows that P_0, P_1 and P_2 will be changed abruptly when the s-characterized feature switches on for the spin-up or spin-down channel. For example, for fcc Ni abrupt variations of P_0, P_1 and P_2 are observed at 0.6 eV below and 0.4 eV above Fermi energy, which is consistent with the switching on of an s-characterized density of states for the spin-up and spin-down channels, respectively.

3.2. Anisotropic $P_{1,i}$ and $P_{2,i}$ for cubic structures

To explore the intrinsic anisotropy of P in both ballistic and diffusive regimes for materials with a cubic structure, we have calculated anisotropic $P_{1,i}$ and $P_{2,i}$ at the Fermi energy for bcc Fe, fcc Co and fcc Ni as a function of crystal direction. The crystal direction, i, varies from [0, 0, 1] to [1, 1, 0] in the $(-1, 1, 0)$ plane and from [1, 1, 0] to [0, 1, 0] in the (0, 0, 1) plane.

3.2.1. $P_{2,i}$ for bcc Fe, fcc Co and fcc Ni. In all directions, $P_{2,i}$ exhibits constant values of 33.1%, 21.7% and 10.8% for bcc Fe, fcc Co and fcc Ni, respectively. The values of anisotropic $P_{2,i}$ are the same as the corresponding isotropic P_2. So, $P_{2,i}$ shows an isotropic feature. According to (2) and (4), $P_{2,i}$ is a function of $\langle Nv_i^2\rangle_\sigma$. For a physical v_i^2 dependent parameter, as proved analytically in the appendix, its integration over the whole Fermi surface should be a constant for a material with cubic symmetry. Therefore, the isotropic feature of $P_{2,i}$ results from the combination of its v_i^2 dependence and the cubic symmetry of the crystal structure in bcc Fe, fcc Co and fcc Ni.

3.2.2. $P_{1,i}$ for bcc Fe, fcc Co and fcc Ni. As pointed out in the appendix, if P is not v_i^2 dependent, as in the case of $P_{1,i}$, it will no longer be isotropic. The calculated $P_{1,i}$ for bcc Fe, fcc Co and fcc Ni are shown in the lower parts of figures 3–5, respectively. To investigate how $P_{1,i}$ responds to the variation of the crystal direction, the relevant ballistic conductance of spin-up and spin-down channels as a function of i, $\langle Nv_i\rangle_\uparrow$ and $\langle Nv_i\rangle_\downarrow$ are also plotted in the upper parts of figures 3–5. For bcc Fe as shown in figures 3(c) and (d), the minimum and maximum values of $P_{1,i}$ are found to be 33.4% and 37.7% in the $\langle 0, 0, 1\rangle$ and $\langle 1, 1, 1\rangle$ directions, respectively. For fcc Co and fcc Ni, however, negative values of $P_{1,i}$ are observed in figures 4(c)–(d) and 5(c)–(d), respectively. For fcc Co, the

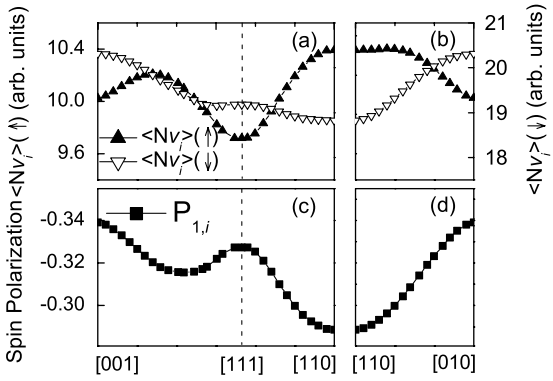

Figure 4. The same as in figure 3, but for fcc Co.

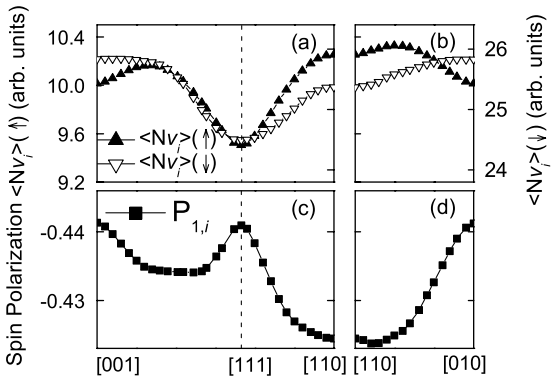

Figure 5. The same as in figure 3, but for fcc Ni.

minimum absolute $P_{1,i}$ value of 28.9% is found in the $\langle 0, 0, 1\rangle$ direction and the maximum one is 33.9% in the $\langle 1, 1, 0\rangle$ direction. The maximum and minimum absolute values of $P_{1,i}$ for fcc Ni are calculated respectively as 44.0% in the $\langle 0, 0, 1\rangle$ and $\langle 1, 1, 1\rangle$ directions and 42.4% in the $\langle 81, 100, 0\rangle$ direction (having an angle of 6 degrees away from their neighboring $\langle 1, 1, 0\rangle$ directions). It should be mentioned that as in the case of the calculation of isotropic P_1 and P_2, a sign reversal is found in the calculation of anisotropic $P_{1,i}$ and $P_{2,i}$ for fcc Co and fcc Ni, but it is absent for bcc Fe.

As regards the $P_{1,i}$ of bcc Fe, fcc Co and fcc Ni, two important features can be obtained. The first one is related to the degree of anisotropy, ω, which is defined by the ratio of the difference between the minimum and maximum absolute $P_{1,i}$ (or $P_{2,i}$) values to the minimum absolute $P_{1,i}$ (or $P_{2,i}$). ω is 0.17 for fcc Co and 0.13 for bcc Fe, which are much larger than that of 0.04 for fcc Ni. The second one is that their extrema appear in different directions for bcc Fe, fcc Co and fcc Ni as mentioned above. According to (2), the absolute value of $P_{1,i}$ is determined by the difference between $\langle Nv_i\rangle_\uparrow$ and $\langle Nv_i\rangle_\downarrow$. Therefore, the two features of $P_{1,i}$ should be derived from the various types of dependence of $\langle Nv_i\rangle_\uparrow$ and $\langle Nv_i\rangle_\downarrow$ on i, which is clearly shown in the upper parts of figures 3–5. For fcc Ni, the direction dependence of $\langle Nv_i\rangle_\uparrow$ is similar to that of $\langle Nv_i\rangle_\downarrow$, which leads to a rather weaker anisotropy of $P_{1,i}$. In contrast, an obvious difference between the direction dependences of $\langle Nv_i\rangle_\uparrow$ and $\langle Nv_i\rangle_\downarrow$ is found for bcc Fe and fcc Co. Taking bcc Fe as a typical example, $\langle Nv_i\rangle_\uparrow$ reaches its maximum in the $\langle 1, 1, 1\rangle$ direction and $\langle Nv_i\rangle_\downarrow$ nearly reaches its minimum in the same directions, which leads to a much stronger anisotropy of $P_{1,i}$. In the same way, the second feature can be explained by considering the direction dependence of ballistic conductance.

In general, a large overlap of conduction electrons between the neighboring atoms gives rise to the widening of the conduction bands and hence a larger electron velocity component in that direction. As a result, the above-mentioned crystal direction dependence of $\langle Nv_i\rangle_\uparrow$ and $\langle Nv_i\rangle_\downarrow$ is determined by orbital extension of the spin-up or spin-down conduction electrons of an atom and the relative positions of its neighboring atoms. In the following paragraph, taking bcc Fe and fcc Ni as an example, we will use this scenario to explain the dependence of $\langle Nv_i\rangle_\uparrow$ and $\langle Nv_i\rangle_\downarrow$ on i.

In the case of fcc Ni, crossing the Fermi level there is one spin-up band with s-character, one spin-down band with s-character and three spin-down bands with d-character [15]. When the s-characterized electrons exist, the ballistic conductance, as well as the anisotropy of $\langle Nv_i\rangle_\uparrow$ and $\langle Nv_i\rangle_\downarrow$, are mainly determined by these s-characterized electrons. The s orbital has an isotropically spherical symmetry and the overlapping of the s orbitals and the ballistic conductance should be determined by the distance between the neighboring atoms. In fcc Ni, the nearest neighboring Ni atom is located in the $\langle 1, 1, 0\rangle$ directions and the second and the third nearest neighboring Ni atoms are located in the $\langle 1, 0, 0\rangle$ and $\langle 1, 1, 1\rangle$ directions, respectively. Therefore, the s orbital overlaps to its greatest degree in the $\langle 1, 1, 0\rangle$ directions and the least degree in the $\langle 1, 1, 1\rangle$ directions. That is why both the smallest $\langle Nv_i\rangle_\uparrow$ and $\langle Nv_i\rangle_\downarrow$ for fcc Ni are observed in the $\langle 1, 1, 1\rangle$ directions and the largest ones are observed near the $\langle 1, 1, 0\rangle$ directions, as shown in figures 5(a) and (b).

In the case of bcc Fe, crossing the Fermi level there are one s-characterized and one d-characterized spin-up bands [15]. $\langle Nv_i\rangle_\uparrow$ of bcc Fe is mainly controlled by the s-characterized electrons. In the bcc structure the nearest, the second and the third nearest neighboring atoms are located in the $\langle 1, 1, 1\rangle$, $\langle 1, 0, 0\rangle$ and $\langle 1, 1, 0\rangle$ directions, respectively. Thus, $\langle Nv_i\rangle_\uparrow$ reaches its maximum and minimum at in the [1, 1, 1] direction and [1, 1, 0] direction, respectively, as shown in the figures 3(a) and (b). On the other hand, there are only four d-characterized spin-down bands crossing the Fermi energy. As no s-characterized band is observed for spin-down conduction electrons, $\langle Nv_i\rangle_\downarrow$ will be determined by the d-characterized electrons with much stronger anisotropy than s-characterized ones. So, the crystal direction dependence of $\langle Nv_i\rangle_\downarrow$ significantly differs from that of $\langle Nv_i\rangle_\uparrow$. It is well known that there are five d orbitals of the xy, yz, zx, $3z^2 - r^2$ and x^2–y^2 symmetries. The d orbitals with xy, yz and zx symmetries have extensions to the directions between the coordinate basis vectors, whereas those with $3z^2$–r^2 and x^2–y^2 symmetries have extension to the directions along the coordinate basis vectors. Three of the four d-characterized spin-down conduction bands have orbitals extending to the directions between the coordinate basis vectors, and one has an orbital extending along the coordinate basis vectors [15]. The extension of these d orbitals leads to stronger electronic overlapping in the $\langle 1, 0, 0\rangle$ and $\langle 1, 1, 0\rangle$ directions and thus

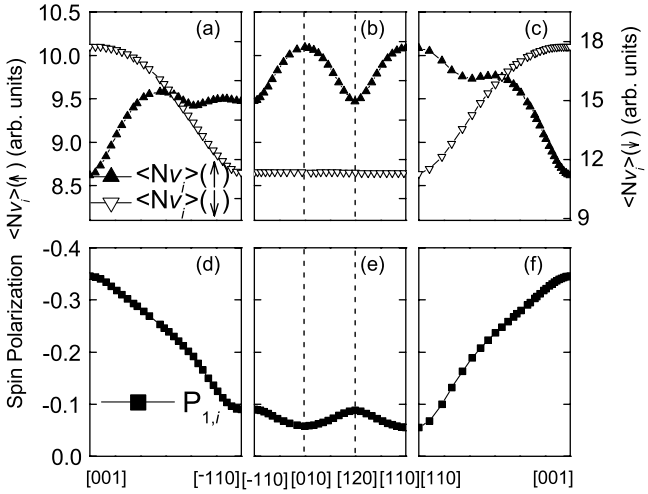

Figure 6. (a)–(c) Spin-up and spin-down ballistic conductance, $\langle Nv_i\rangle_\uparrow$ and $\langle Nv_i\rangle_\downarrow$, as a function of the crystal direction in hcp Co. (d)–(f) Anisotropic $P_{1,i}$ as a function of i in hcp Co.

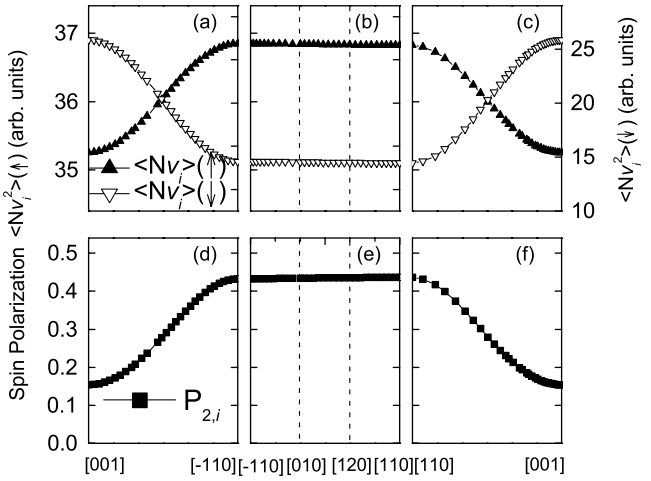

Figure 7. (a)–(c) The same as in figure 6, but for the spin-up and spin-down diffusive conductance, $\langle Nv_i^2\rangle_\uparrow$ and $\langle Nv_i^2\rangle_\downarrow$. (d)–(f) The same as in figure 6, but for the anisotropic $P_{2,i}$.

a larger ballistic conductance in these directions, resulting in nearly the smallest value in the $\langle 1, 1, 1\rangle$ direction as shown in figure 3(a).

3.3. Anisotropic $P_{1,i}$ and $P_{2,i}$ for hcp Co with noncubic structure

In the noncubic materials, the transport properties exhibit rather anisotropic character experimentally and theoretically [18], which is ascribed to the breaking down of the cubic symmetry of the Fermi surface and the anisotropic distribution of the electronic velocity vectors in real space [18]. So we expect a kind of anisotropy of P induced by the breaking down of the cubic symmetry. To that end, we take hcp Co as an example and calculate $P_{1,i}$ and $P_{2,i}$ as a function of i. i ranges from [0, 0, 1] to [1, 1, 0] in the $(-1, 1, 0)$ plane, from [1, 1, 0] to $[-1, 1, 0]$ in the (0, 0, 1) plane and from $[-1, 1, 0]$ to [0, 0, 1] in the (1, 1, 0) plane in the hcp structure.

In figures 6 and 7, the results for $P_{1,i}$ and $P_{2,i}$ of hcp Co are shown respectively. Figures 6(d)–(f) show that negative values are observed for $P_{1,i}$ in all directions. The minimum and maximum absolute values of 5.8% and 34.5% are found in the $\langle 0, 1, 0\rangle$ and $\langle 0, 0, 1\rangle$ directions, respectively. A small but appreciable anisotropy of $P_{1,i}$ is also found in the (0, 0, 1) plane. On the contrary, positive values of $P_{2,i}$ are observed, as shown in the figures 7(d)–(f). The minimum and maximum values of 15.4% and 43.4% are obtained in the $\langle 0, 0, 1\rangle$ direction and in the (0, 0, 1) plane, respectively. Comparing the results in figures 7(d)–(f) with those in figures 6(d)–(f), almost the same values of $P_{2,i}$ are found in the (0, 0, 1) plane in contrast to the case of $P_{1,i}$. In addition, as in the case of the cubic materials mentioned above, the sign reversal from $P_{1,i}$ to $P_{2,i}$ for hcp Co is also derived from the s-character of the spin-up electrons and the d-character of the spin-down ones at the Fermi energy, as indicated in the spin polarized density of states for hcp Co in figure 2. The anisotropy of $P_{1,i}$ is stronger than that of $P_{2,i}$ in the (0, 0, 1) plane, due to the much stronger anisotropy of $\langle Nv_i\rangle_\uparrow$ in this plane, as shown in figures 6(a)–(c) and 7(a)–(c).

Most importantly, in contrast to the case of fcc Co, much stronger anisotropy is observed for both $P_{1,i}$ and $P_{2,i}$ of hcp Co. For $P_{1,i}$ of hcp Co, ω is 5.95, much larger than the corresponding 0.17 of fcc Co. On the other hand, in contrast to the isotropic feature of $P_{2,i}$ in fcc Co, ω is 2.82 for $P_{2,i}$ in hcp Co. Figures 6(a)–(c) and 7(a)–(c) show that the dependence of $\langle Nv_i\rangle_\uparrow$ (and $\langle Nv_i^2\rangle_\uparrow$) on crystal direction differs largely from that of $\langle Nv_i\rangle_\downarrow$ (and $\langle Nv_i^2\rangle_\downarrow$). $\langle Nv_i\rangle_\uparrow$ and $\langle Nv_i^2\rangle_\uparrow$ reach their minimum in the $\langle 0, 0, 1\rangle$ directions (maximum in the (0, 0, 1) plane), $\langle Nv_i\rangle_\downarrow$ and $\langle Nv_i^2\rangle_\downarrow$ reach their maximum (minimum) in the same directions. In addition, from the spin polarized density of states of hcp Co in figure 2, s-characterized conductive electrons and d-characterized ones are observed for spin-up and spin-down channels, respectively. Because the anisotropy of the orbital extension of the d orbital is stronger than that of the s orbital, the variation of $\langle Nv_i\rangle_\downarrow$ (and $\langle Nv_i^2\rangle_\downarrow$) with i is much greater than that of $\langle Nv_i\rangle_\uparrow$ (and $\langle Nv_i^2\rangle_\uparrow$), which can be seen in figures 6(a)–(c) and 7(a)–(c). According to (2), the large anisotropy of $P_{1,i}$ ($P_{2,i}$) in hcp Co is mainly derived from the anisotropy of $\langle Nv_i\rangle_\downarrow$ (and $\langle Nv_i^2\rangle_\downarrow$).

4. Conclusion

We have presented a general approach to evaluating with high accuracy the anisotropic degree of transport spin polarization in the ballistic regime, $P_{1,i}$ and in the diffusive regime, $P_{2,i}$. Its validity is confirmed in the case for the isotropic degree of transport spin polarization in bcc Fe and fcc Ni by comparison with previous results. Considering the anisotropic distribution of the electronic velocity vectors in real space, $P_{1,i}$ and $P_{2,i}$, as functions of crystal direction, can be deduced according to the band structures of bcc Fe, fcc Co, fcc Ni and hcp Co. For cubic crystal structures, $P_{1,i}$ shows a small but appreciable anisotropy, due to the difference in the electronic orbital extension for spin-up and spin-down conduction bands. Meanwhile, $P_{2,i}$ shows an isotropic feature, which is a result of

the combination of its v_i^2 dependence and the cubic symmetry. Noticeably, due to the breaking down of the cubic symmetry of the crystal in hcp Co, both $P_{1,i}$ and $P_{2,i}$ show a strong anisotropy and the value of ω reaches 5.95 for $P_{1,i}$ and 2.82 for $P_{2,i}$. The large anisotropy of $P_{1,i}$ ($P_{2,i}$) in hcp Co mainly results from the anisotropy of spin-down ballistic (diffusive) conductance, i.e. $\langle Nv_i\rangle_\downarrow$ (and $\langle Nv_i^2\rangle_\downarrow$). In one word, we have got the intrinsic anisotropy of the degree of transport spin polarization. This is important for a better understanding of the spin dependent transport properties of a ferromagnetic material.

Acknowledgments

This work was supported by the National Natural Science Foundation of China grant no. 50531010, and the Research Grants Council of Hong Kong.

Appendix

For a material with cubic crystal structure, the integration of a physical parameter proportional to v_i^2 over the whole Fermi surface will be proved constant, i.e. such a parameter is independent of the i direction. For a cubic structure, the energy distribution for a given energy band in reciprocal space satisfies the following relations:

$$\begin{aligned} E &= E(\pm k_1, \pm k_2, \pm k_3) \\ &= E(\pm k_1, \pm k_3, \pm k_2) \\ &= E(\pm k_2, \pm k_1, \pm k_3) \\ &= E(\pm k_2, \pm k_3, \pm k_1) \\ &= E(\pm k_3, \pm k_2, \pm k_1) \\ &= E(\pm k_3, \pm k_1, \pm k_2) \end{aligned} \tag{A.1}$$

where $E(k_1, k_2, k_3)$ stands for the electronic energy at $\boldsymbol{k}(k_1, k_2, k_3) = k_1\boldsymbol{k}_x + k_2\boldsymbol{k}_y + k_3\boldsymbol{k}_z$. If $E = E_0$, an isosurface can be obtained, and if E_0 equals to the Fermi energy, this isosurface is the Fermi surface. If $\boldsymbol{k}(k_1, k_2, k_3)$ is on the Fermi surface, the k-points of $\boldsymbol{k}(-k_1, -k_2, -k_3)$, $\boldsymbol{k}(\pm k_1, \pm k_3, \pm k_2)$, $\boldsymbol{k}(\pm k_2, \pm k_1, \pm k_3)$, $\boldsymbol{k}(\pm k_2, \pm k_3, \pm k_1)$, $\boldsymbol{k}(\pm k_3, \pm k_2, \pm k_1)$ and $\boldsymbol{k}(\pm k_3, \pm k_1, \pm k_2)$ should also be on the Fermi surface.

In the following part, firstly we will deduce the relations between the electronic velocity vectors of these 48 equivalent k-points. Because of the fact that the equivalent points are connected by symmetry operations (which correspond to rotations and reflections) and rotations and reflections of a vector are orthogonal transformations, the energy gradients at these equivalent k-points have the same lengths. Therefore, the velocity vector, which is proportional to the energy gradient in the reciprocal space, has the same absolute value, $|v|$, for all the 48 equivalent k-points.

Next, we will prove that the integration of a physical parameter proportional to v_i^2 over the whole Fermi surface is constant. Given a crystal direction i, $\boldsymbol{r}_i = \cos\theta_1\boldsymbol{r}_x + \cos\theta_2\boldsymbol{r}_y + \cos\theta_3\boldsymbol{r}_z$ ($\cos^2\theta_1 + \cos^2\theta_2 + \cos^2\theta_3 = 1$), the integration can be written as follows in the summation form:

$$\langle v_i^2\rangle = \sum_{k\in \mathrm{FS}} [\boldsymbol{v}(k_1, k_2, k_3)\cdot\boldsymbol{r}_i]^2 \tag{A.2}$$

where FS stands for the Fermi surface. If the Fermi surface is divided into $48n$ parts and then classified into n groups and there are 48 equivalent k-points in each group, the summation form can be written as the summation of n terms as

$$\sum_{k\in \mathrm{G}_n} [\boldsymbol{v}(k_1, k_2, k_3)\cdot\boldsymbol{r}_i]^2 \tag{A.3}$$

where G_n denotes the nth group. As for the k-point group, $\boldsymbol{k}(\pm k_1, \pm k_2, \pm k_3)$, $\boldsymbol{k}(\pm k_1, \pm k_3, \pm k_2)$, $\boldsymbol{k}(\pm k_2, \pm k_1, \pm k_3)$, $\boldsymbol{k}(\pm k_2, \pm k_3, \pm k_1)$, $\boldsymbol{k}(\pm k_3, \pm k_2, \pm k_1)$ and $\boldsymbol{k}(\pm k_3, \pm k_1, \pm k_2)$, for example, the relevant summation term can be expressed as:

$$\begin{aligned} &\sum_{k\in \mathrm{G}_n} [\boldsymbol{v}(k_1, k_2, k_3)\cdot\boldsymbol{r}_i]^2 \\ &= 4\big\{[\boldsymbol{v}(k_1, k_2, k_3)\cdot\boldsymbol{r}_i]^2 + [\boldsymbol{v}(k_2, k_3, k_1)\cdot\boldsymbol{r}_i]^2 \\ &\quad + [\boldsymbol{v}(k_3, k_1, k_2)\cdot\boldsymbol{r}_i]^2 + [\boldsymbol{v}(-k_1, k_2, k_3)\cdot\boldsymbol{r}_i]^2 \\ &\quad + [\boldsymbol{v}(-k_2, k_3, k_1)\cdot\boldsymbol{r}_i]^2 + [\boldsymbol{v}(-k_3, k_1, k_2)\cdot\boldsymbol{r}_i]^2 \\ &\quad + [\boldsymbol{v}(k_1, -k_2, k_3)\cdot\boldsymbol{r}_i]^2 + [\boldsymbol{v}(k_2, -k_3, k_1)\cdot\boldsymbol{r}_i]^2 \\ &\quad + [\boldsymbol{v}(k_3, -k_1, k_2)\cdot\boldsymbol{r}_i]^2 + [\boldsymbol{v}(-k_1, -k_2, k_3)\cdot\boldsymbol{r}_i]^2 \\ &\quad + [\boldsymbol{v}(-k_2, -k_3, k_1)\cdot\boldsymbol{r}_i]^2 + [\boldsymbol{v}(-k_3, -k_1, k_2)\cdot\boldsymbol{r}_i]^2\big\} \\ &= 16(v_1^2 + v_2^2 + v_3^2) = 16|v|^2. \end{aligned} \tag{A.4}$$

That is to say, each of the n summation terms in (A.3), as well as the value of whole (A.3), show constant values and are independent of i. So far, we have proved that the integration of a physical parameter proportional to v_i^2 over all the Fermi surface is constant and independent of the i direction.

Finally, we would like to emphasis that the isotropic feature of such a physical parameter originates from its v_i^2 dependence and the cubic symmetry of the crystal structure, which leads to a complete cancelation of the interaction term in the scalar products in (A.4). But, for a v_i dependent physical parameter, such an integration can not be i independent any more because the interaction term can not be canceled out after the summation. Therefore, for a physical parameter proportional to v_i, its integration will not be a constant value for all crystal directions.

References

[1] Baibich M N, Broto J M, Fert A, Nguyen Van Dau F, Petroff F, Eitenne P, Creuzet G, Friederich A and Chazelas J 1988 *Phys. Rev. Lett.* **61** 2472
[2] Binasch G, Grünberg P, Saurenbach F and Zinn W 1989 *Phys. Rev.* B **39** 4828
[3] Meservey R and Tedrow P M 1994 *Phys. Rep.* **238** 173
[4] Wolf S A, Awschalom D D, Buhrman R A, Daughton J M, von Molnar S, Roukes M L, Chtchelkanova A Y and Treger D M 2001 *Science* **294** 1488
[5] Moodera J S, Kinder Lisa R, Wong Terrilyn M and Meservey R 1995 *Phys. Rev. Lett.* **74** 3273
[6] Katine J A, Albert F J, Buhrman R A, Myers E B and Ralph D C 2000 *Phys. Rev. Lett.* **84** 3149
[7] Jaffrès H and Fert A 2002 *J. Appl. Phys.* **91** 8111
[8] Soulen R J Jr, Byers J M, Osofsky M S, Nadgorny B, Ambrose T, Cheng S F, Broussard P R, Tanaka C T, Nowak J, Moodera J S, Barry A and Coey J M D 1998 *Science* **282** 85
[9] de Groot R A, Mueller F M, van Engen P G and Buschow K H J 1983 *Phys. Rev. Lett.* **50** 2024

[10] Ishida S, Masaki T, Fujii S and Asano S 1998 *Physica* B **245** 1
[11] Schwarz K 1986 *J. Phys. F: Met. Phys.* **16** L211
[12] Yanase A and Siratori K 1984 *J. Phys. Soc. Japan* **53** 312
[13] Johnson P D 1997 *Rep. Prog. Phys.* **60** 1217
[14] Meservey R and Tedrow P M 1994 *Phys. Rep.* **238** 173
[15] Mazin I I 1999 *Phys. Rev. Lett.* **83** 1427
[16] Sharvin Yu V 1965 *Zh. Eksp. Teor. Fiz.* **48** 984
Sharvin Yu V 1965 *Sov. Phys.—JETP* **21** 655 (Engl. Transl.)
[17] Allen P B 1978 *Phys. Rev.* B **17** 3725
[18] Sanborn B A, Allen P B and Papaconstantopoulos D A 1989 *Phys. Rev.* B **40** 6037
[19] Schep Kees M, Kelly Paul J and Bauer Gerrit E W 1998 *Phys. Rev.* B **57** 8907
[20] Velev J, Sabirianov R F, Jaswal S S and Tsymbal E Y 2005 *Phys. Rev. Lett.* **94** 127203
[21] Xu P X, Xia K, Zwierzycki M, Talanana M and Kelly P J 2006 *Phys. Rev. Lett.* **96** 176602
[22] Bahramy M S, Murugan P, Das G P and Kawazoe Y 2007 *Phys. Rev.* B **75** 054404
[23] Lorensen W and Cline H 1987 *Comput. Graph.* **21** 163
[24] Kokalj A 2003 *Comput. Mater. Sci.* **28** 155
[25] Wimmer E, Krakauer H, Weinert M and Freeman A J 1981 *Phys. Rev.* B **24** 864
[26] Weinert M, Wimmer E and Freeman A J 1982 *Phys. Rev.* B **26** 4571